


Research Article

Investigation of the Properties of Metakaolin-Based Geopolymer Materials Using Ferrisilicates as Additives Synthesised in Sodium Hydroxide Solution or Distilled Water

Franklin Kenne Tazune¹, Lucile Dolly Dedzo Nzangue¹, Alexis Ngueteu Kamlo², Hervé Kouamo Tchakouté^{1, 3*} , Claus Henning Rüschert³

¹Laboratory of Analytical Chemistry, Faculty of Science, Department of Inorganic Chemistry, University of Yaounde I, P.O. Box 812, Yaounde, Cameroon

²Department of Chemistry, Higher Teacher Training College, University of Yaounde I, 4124 Yaounde, P.O. Box 47, Cameroon

³Institute of Mineralogy, Leibniz University Hanover, Callinstrasse 3, D-30167 Hanover, Germany
Email: hervetchakoute@gmail.com

Received: 31 October 2023; **Revised:** 27 December 2023; **Accepted:** 8 January 2024

Abstract: The main objective of this work is to investigate the behaviour of ferrisilicates prepared from hematite and two silica sources (rice husk ash and silica fume) on the compressive strength of geopolymer materials. Some ferrisilicates were synthesised in 2 M sodium hydroxide solution, while others were prepared using distilled water as a solvent. The $\text{Fe}_2\text{O}_3/\text{SiO}_2$ molar ratio contained in the ferrisilicates was set to 0.2. Metakaolin and sodium silicate solution with a molar ratio of $\text{SiO}_2/\text{Na}_2\text{O}$ of 1.6 were used as the aluminosilicate and hardener in this work. The control geopolymer compressive strength is 53.34 MPa. For ferrisilicates prepared in alkaline solution using rice husk ash and silica fume, their compressive strength values are 71.91 and 77.72 MPa, respectively. The compressive strengths of the geopolymer materials made from ferrisilicates prepared in distilled water using rice husk ash and silica fume are 74.13 and 44.73 MPa, respectively. In the presence of ferrisilicate obtained by dissolving silica fume and hematite in sodium hydroxide solution, the maximum compressive strength of 77.72 MPa was obtained. When ferrisilicates from the mixture of silica fume, hematite, and distilled water were used as an additive, the minimum compressive strength of 43.73 MPa is achieved. It can be concluded that additives synthesised in an alkaline medium and those obtained in distilled water with rice husk ash improve compressive strength. On the other hand, the compressive strength of the geopolymer material that uses the additive produced with silica fume in distilled water is lower (44.73 MPa).

Keywords: hematite, silica sources, ferrisilicates, metakaolin, geopolymer materials, compressive strength

1. Introduction

Geopolymer materials are obtained at room temperature by depolymerisation of semi-crystalline aluminosilicate sources with a chemical reagent or hardener. This is followed by a polycondensation reaction between the aluminate and silicate species formed. A sodium or potassium silicate solution and phosphoric acid can be used as hardeners in the synthesis of geopolymer materials. It is important to note that a sodium silicate solution, known as sodium water glass, is the hardener generally used by several researchers to prepare geopolymer materials. Although the compressive

strength of the geopolymer materials obtained by some researchers is higher than that of Portland cement, others have attempted to improve the properties by adding certain compounds to the aluminosilicate source or by replacing these aluminosilicates with other minerals [1]-[3]. For example, Mabah et al. [4] investigated how semi-crystalline calcium silicate hydrate influences compressive strength in geopolymer materials from metakaolin. They reported that as the content of semi-crystalline calcium silicate hydrate in the metakaolin increased from 0 to 10 wt%, the compressive strength of the geopolymer materials increased from 37 to 51 MPa. Tchakouté et al. [5] investigated the effect of microcomposites on the compressive strength of geopolymer materials and obtained the maximum compressive strength of around 69 MPa when metakaolin was replaced by 10 wt% of microcomposite. The effects of calcium aluminate hydrate synthesis on the properties of metakaolin-based geopolymer composites were investigated by Moudio et al. [6]. They concluded that when metakaolin is replaced by 10 wt% calcium aluminate hydrate, the maximum compressive strength of the final product is approximately 64 MPa. In contrast, Riyap et al. [7] investigated the compressive strength of geopolymer materials resulting from the addition of partially crystalline alumina to metakaolin and waste-fired clay brick. It is important to note that metakaolin is rich in quartz and waste-fired brick is rich in amorphous silica. They reported increasing the compressive strength of metakaolin-based geopolymer composites from 36 to 55 MPa. As the amount of semi-crystalline alumina increases, those of waste-fired clay brick decrease from 48 to 20 MPa. Eggshell, bauxite, and rice husk ash are used as sources of calcium, alumina, and silica, respectively, for the preparation of additives. The effect of different iron minerals such as hematite, magnetite, and goethite on the compressive strength of geopolymer cement was investigated by Ngnintedem et al. [8]. It was reported that a 10 wt% addition of hematite to metakaolin resulted in a compressive strength of 56 MPa. Kaze et al. [9] and Kamseu et al. [10] investigated the microstructure and engineering properties of geopolymer composites made from a mixture of laterite and rice husk. The first authors observed the formation of ferrisilicate in the structure of geopolymer composites. They reported that the formation of ferrisilicate in the structure of geopolymer composites changed their flexural strength and microstructure. The second reported that, through the formation of Fe-O-Si bonds, the presence of ferrisilicates in the structure of geopolymer materials contributes to the increase in compressive strength values. Ferrisilicates are formed under hydrothermal conditions at temperatures between 50 and 200 °C, according to Zhu et al. [11] and Hensen et al. [12]. We believe an iron source (such as hematite) and silica sources (such as rice husk ash and silica fume) could be used to produce this mineral. Hematite ($\alpha\text{-Fe}_2\text{O}_3$) is one of the most abundant minerals in the Earth's crust [13]. Acknowledged as an important material for various sciences, the ore's high resistance to corrosion and widespread availability has attracted researchers' attention [14]. Silica fume is amorphous microsilica. It is a polymorphic form of silicon dioxide. Adak et al. [15], Duan et al. [16], Saini and Vattipalli [17], and Liu et al. [18] incorporated silica fume into the structure of geopolymer composites. They concluded that the geopolymer composites had lower porosity and water absorption. Liu et al. [18] reported that when 30 wt% silica fume was incorporated into the structure of fly ash/slag-based geopolymer concretes, the compressive strength reached 151 MPa. In view of the above, ferrisilicates can be synthesised from hematite and silica fume or rice husk ash. They can be used as additives to improve the properties of geopolymer composites.

The purpose of the present work is to investigate the behaviour of ferrisilicates from the mixture of hematite and two silica sources (silica fume and rice husk ash) on the compressive strength of geopolymer materials. The ferrisilicates were prepared separately using sodium hydroxide solution (2M) and distilled water as solvents. A commercially available solution of sodium silicate with a molar ratio of SiO_2 to Na_2O equal to 1.6 was used as the hardener. Compressive strength measurements were used to investigate the behaviour of the synthesised ferrisilicates within the geopolymer structure. The minerals in these materials have been identified by X-ray diffraction analysis. The functional groups were monitored using infrared spectroscopy and the fragments of geopolymer materials were observed using scanning electron microscopy and energy dispersive X-ray spectroscopy (EDS) mapping.

2. Materials and experimental methods

2.1 Materials

The kaolin used in this study came from the Mayouom site in the West Region of Cameroon. The collected kaolin was air-dried for at least 24 hours and pulverised for 1 hour in a ball mill (MGS, Srl) to obtain kaolin (MY3) powder.

Metakaolin, designated MK-MY3, was obtained by calcining kaolin powder in a programmable electric furnace at 700 °C for 4 h at a heating and cooling rate of 5 °C/min. The iron source in the form of hematite, designation F, was supplied by Serraciments Company (Barcelona, Spain). This iron oxide has been used by Ngintedem et al. [8] as an additive for the synthesis of geopolymer materials. They reported that the broadening of the peak shows that the average size of the crystals of hematite is 120 nm. The Upper Nyong Valley Development Association (UNVDA) provided rice husk ash (RHA), a known source of silica. This company calcined rice husk at 600 °C in a traditional kiln to obtain white rice husk ash. This ash is already being used by several researchers [4], [5], [19]. The other silica source used was commercially available silica fume (SF) with the chemical formula $\text{SiO}_2 \cdot x\text{H}_2\text{O}$ (Merck, No 10 279-57-9). Silica fume has been used by Melele et al. [19] for the preparation of sodium water glass. They reported that the specific surface area of silica fume is $169.84 \pm 2.05 \text{ m}^2/\text{g}$ and Tchakouté et al. [5] reported that the one of rice husk ash is $4.08 \pm 0.06 \text{ m}^2/\text{g}$. Laboratory-grade granules (96 wt%, Sigma Aldrich, Italy) were used as NaOH pellets. The hardener used was sodium silicate with a $\text{SiO}_2/\text{Na}_2\text{O}$ molar ratio of 1.6. This solution was provided by Ingessil. The company is based in Verona, Italy. X-ray patterns and infrared spectra of rice husk ash (RHA) and silica fume (SF) are shown in Figures 1 and 2. The chemical composition of kaolin and rice husk ash is shown in Table 1.

Table 1. Chemical compositions of kaolin (MY3) and rice husk ash (RHA), wt%

Oxides	Samples	
	MY3	RHA [4], [19]
MgO	-	0.28
Al ₂ O ₃	33.29	0.58
SiO ₂	46.61	93.20
K ₂ O	0.94	3.05
CaO	-	0.57
TiO ₂	3.96	0.03
SO ₂	0.05	-
Fe ₂ O ₃	1.46	2.20
P ₂ O ₅	0.40	-
Others	-	1.78
LOI	13.97	1.2

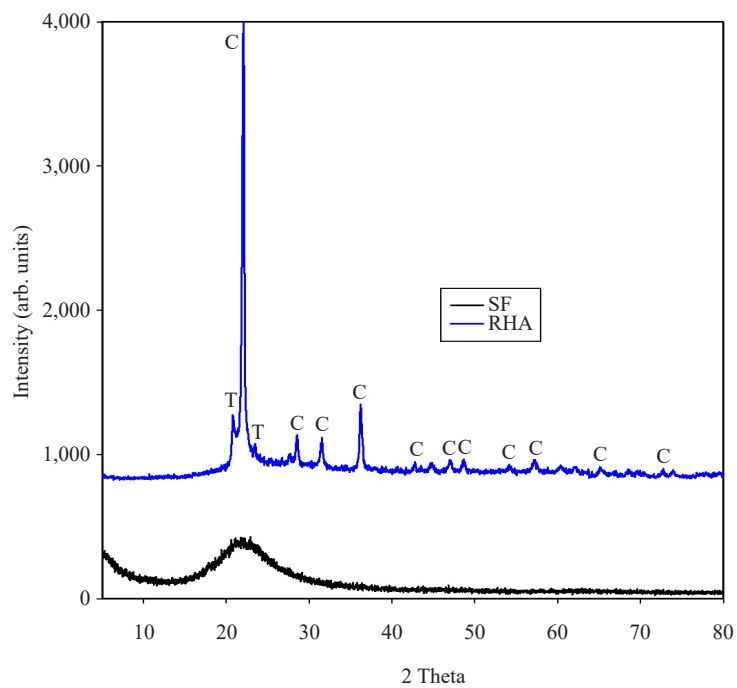


Figure 1. X-ray patterns of rice husk ash (RHA) and silica fume (SF). T and C denote the peaks of tridymite and cristobalite, respectively

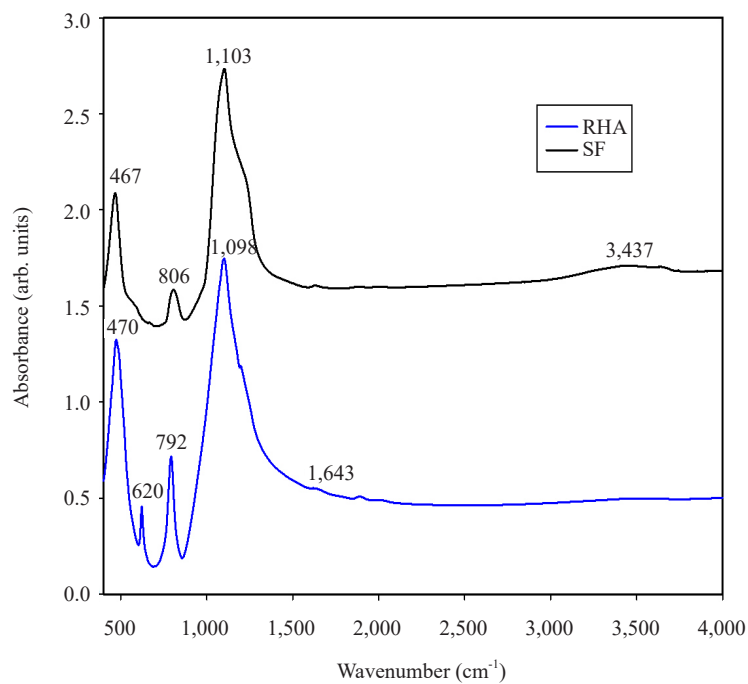


Figure 2. Infrared spectra of rice husk ash (RHA) and silica fume (SF)

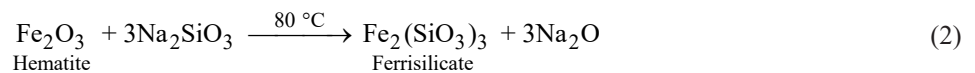
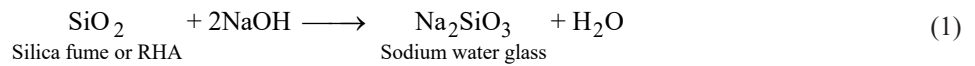
2.2 Experimental methods

2.2.1 Preparation of ferrisilicates

In sodium hydroxide solution with a molarity of 2M and distilled water as the solvent, ferrisilicates with a $\text{Fe}_2\text{O}_3/\text{SiO}_2$ molar ratio set at 0.2 were prepared.

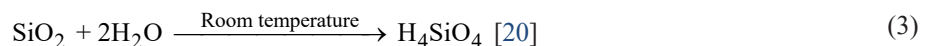
2.2.1.1 In the sodium hydroxide (2M)

The sodium hydroxide solution with a molarity of 2M was prepared by the dissolution of sodium hydroxide pellets in distilled water. The solution obtained was added separately to rice husk ash and silica fume to obtain sodium silicate from rice husk ash and silica fume, respectively. The hematite was then mixed separately with both sodium silicates. The result was two ferrisilicate gels. To ensure homogeneity, each gel was mixed for 5 minutes in a ball mill. The gels obtained were hardened in an oven (GenLabPrime) at 80 °C for 24 hours and the agglomerate materials obtained were pulverised in a ball mill for 5 minutes. The ferrisilicate powders obtained from rice husk ash were named FNR and the one obtained from silica fume was named FNS. The following equations show the preparation of these ferrisilicates in sodium hydroxide:

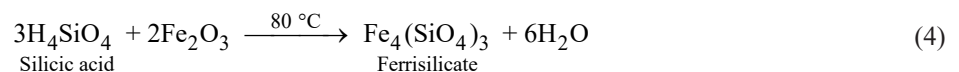


2.2.1.2 In distilled water

The ferrisilicates were synthesised by adding distilled water to rice husk ash or silica fume. Hematite was added to each gel and each gel was then mixed in a ball mill for 5 minutes. The gels obtained were subjected to the same treatment as those obtained with a solution of sodium hydroxide. The ferrisilicate powders from rice husk ash and silica fume were named FR and FS, respectively. The following equations represent the synthesis of these ferrisilicates in distilled water:



This first step is denoted by the hydrolysis reaction.



2.2.2 Synthesis of metakaolin-based geopolymer materials

A metakaolin-based geopolymer material without the addition of ferrisilicate was prepared by adding 240 g of metakaolin with 199.2 g of hardener. The metakaolin-based geopolymer composites were synthesised by adding 240 g of metakaolin to 24 g of each ferrisilicate. Each powder of metakaolin-ferrisilicate was mixed with 219.12 g of hardener for 5 minutes. The resulting pastes were poured into cubic moulds (40 × 40 × 40 mm) and kept at room temperature in the laboratory for 24 hours before demoulding. The demoulded specimens were sealed in plastic bags and left in the laboratory for 28 days before they were tested for their compressive strength. The control metakaolin-based geopolymer was designated GF0. GFNR, GFNS, GFR, and GFS are used for those containing FNR, FNS, FR, and FS, respectively.

2.3 Methods of characterization of raw materials, ferrisilicates, and metakaolin-based geopolymer composites

X-ray diffraction (XRD) and Fourier Transform Infrared (FTIR) spectroscopy were used to characterise the powders of ferrisilicate and metakaolin-based geopolymer composites. The cubic shapes of the metakaolin-based geopolymer composites were used to measure compressive strength and the fragments obtained were used for morphology observation by scanning electron microscopy (SEM) analysis.

The compressive strength values of the metakaolin-based geopolymer composites were determined after 28 days on specimens sealed in plastic and maintained at room temperature in the laboratory in accordance with DIN 1164. In accordance with DIN 1164, the compressive strength values of the metakaolin-based geopolymer composites were determined after 28 days on specimens sealed in plastic bags and stored at room temperature in the laboratory. Once the compressive strengths had been measured, the fragments were collected and a part of them was finely ground in the porcelain mortar and the other part was used to study their morphologies.

The X-ray pattern of each sample was registered on a Bruker D8 Advance equipped with a LynXeye XE T detector, which detects $\text{CuK}\alpha_{1,2}$ in the Bragg-Brentano geometry with a 2θ range covering between 5 and 80° for 1 h with steps of $0.01^\circ 2\theta$. The crystalline phases have been identified with the aid of X'Pert HighScore Plus software.

The KBr method was used to record the spectra of the samples. This was done on the Bruker Vertex 80v. Approximately 200 mg of KBr and 1 mg of each sample were used to prepare each pellet. The whole thing was mixed in an agate mortar and then pressed with a hydraulic press at a force of 110 kN (ENERPAC P392, USA). Spectra of each sample were acquired with 2 cm^{-1} resolution and 16 scans, and data were acquired with OPUS software.

The TG, dTG, and DSC analyses of the kaolin powder were carried out using an alumina crucible between 23 and $1,000^\circ\text{C}$ (technical air with a flow rate of 20 ml/min, a heating/cooling rate of $10^\circ\text{C}/\text{min}$, Setaram Setsys Evolution 1,650).

A Jeol XFlash 6160 Bruker scanning electron microscope (SEM) equipped with energy dispersive X-ray spectroscopy (EDS) using the secondary electron imaging (SEI) mode as the accelerating voltage at 15 kV emission 56.6 μA , probe current 9 and working distance (WD) 8.0 mm was used to study the microscopic morphology and elemental mapping of the geopolymer materials GF0, GFNR, GFNS, GFR, and GFS. Before viewing the images, the samples were coated with a thin layer of gold (sputtered) to avoid distorted backscattered images and to allow the electron accumulation on the examined surface to be discharged.

3. Results and discussion

3.1 Characterizations of raw materials and prepared ferrisilicates

3.1.1 Mineralogical compositions

The X-ray patterns of kaolin (MY3) and metakaolin (MK-MY3) obtained by calcination of MY3 at 700°C are depicted in Figure 3. Peaks of kaolinite, quartz, illite, and anatase can be seen on the X-ray pattern of the kaolin. This figure shows that calcination of kaolin at 700°C for 4 hours causes the disappearance of the kaolinite peaks and the appearance of the broad hump structure located between 13 and $35^\circ (2\theta)$ on the X-ray pattern of metakaolin. The broad hump structure corresponds to the formation of an amorphous aluminosilicate known as metakaolinite. On the X-ray pattern of metakaolin after calcination, the peaks of other minerals such as illite, quartz, and anatase remain unchanged. The peak of kaolinite appearing at d-spacing 3.57 \AA on the X-ray pattern of kaolin (MY3) overlaps with that of anatase. As can be seen in Figure 3, after calcination, this peak shift to the d-spacing of 3.61 \AA corresponds to the main peak of anatase on the X-ray pattern of metakaolin (MK-MY3).

Thermogravimetric Analysis (TGA) and Differential Scanning Calorimetry (DSC) curves of kaolin (MY3) are shown in Figure 4. There are two weight losses with maximum temperatures around 59 and 519°C in the TGA curve. A weak endothermic peak on the DSC curve corresponds to the first weight loss at about 59°C . This is caused by free water molecules evaporating from the surface of the raw material. The dehydroxylation of kaolinite leading to the formation of metakaolinite (equation 5) is responsible for the second weight loss, which corresponds to a strong endothermic peak at about 519°C . This confirms the presence of kaolinite on the X-ray pattern of kaolin (MY3).

The result confirms the presence of the broad hump structure between 13° and 35° (2θ) on the X-ray pattern of the metakaolin (MK-MY3). The faint peak appearing on the DSC curve at about 570 °C is attributed to the polymorphic transformation of α-quartz to β-quartz. The presence of this phenomenon is confirmed by the quartz peaks observed on the X-ray patterns of kaolin and metakaolin (Figure 3). On the DSC curve, at around 985 °C, an exothermic phenomenon is observed. The presence of this phenomenon corresponds to the transformation of metakaolinite into cubic Al-Si spinel phase [21]-[24], see equation 6).

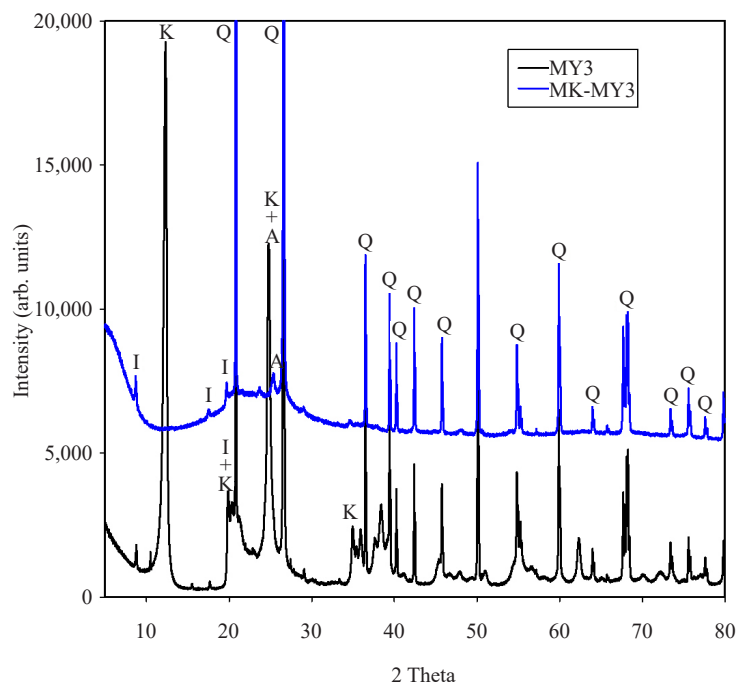
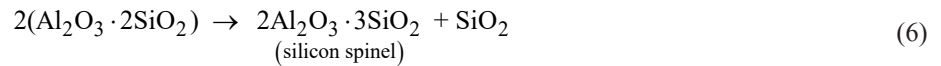
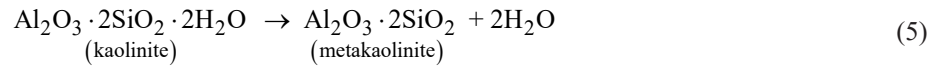


Figure 3. X-ray patterns of kaolin (MY3) and metakaolin (MK-MY3). I, K, A, and Q denote peaks of illite, kaolinite, anatase, and quartz, respectively

The X-ray patterns of different ferrisilicates (FNR, FNS, FR, and FS) are reported in Figure 5. The peaks of commercial hematite are compared to the peaks appearing on the X-ray patterns of various ferrisilicates. Cristobalite and tridymite peaks which originate from rice husk ash are seen on the X-ray patterns of ferrisilicates (FR and FNR) (Figure 1). In addition to these crystalline phases, the X-ray patterns of all ferrisilicates show the peaks of hematite and a broad hump structure corresponding to the amorphous phases contained in their networks. The broad hump structure appears between 14 and 28° (2θ) on the X-ray patterns of ferrisilicates from silica fume and between 17 and 24° (2θ) on the diffractogram of ferrisilicates from rice husk ash. On the other hand, on the X-ray patterns of silica fume and rice husk ash, they were observed from 14 to 32° (2θ) and from 19 to 24° (2θ), respectively. According to Li et al [25], these halo diffractions shifted to lower 2θ, indicating increased pore size in the prepared ferrosilicate structures. Increasing the pore size in the structure of ferrisilicates provides additional nucleation sites in their networks, which could lead to an increase in the polycondensation process. The broad hump structure is more pronounced in the structure of silica fume

(FS and FNS). This corresponds to the higher proportion of the amorphous phase. This could be due to the completely amorphous nature of silica fume (Figure 1).

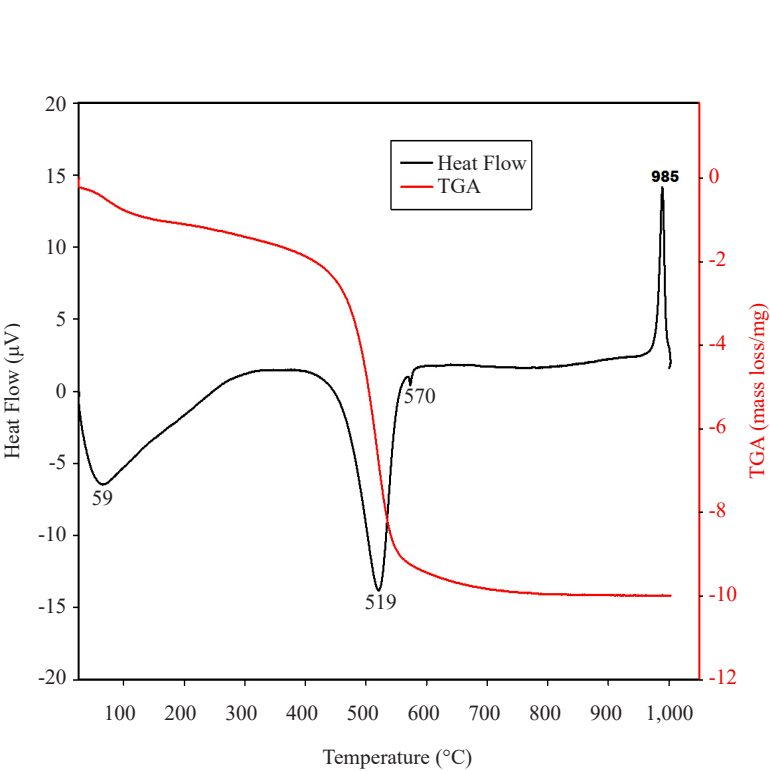


Figure 4. TGA and DSC curves of kaolin MY3

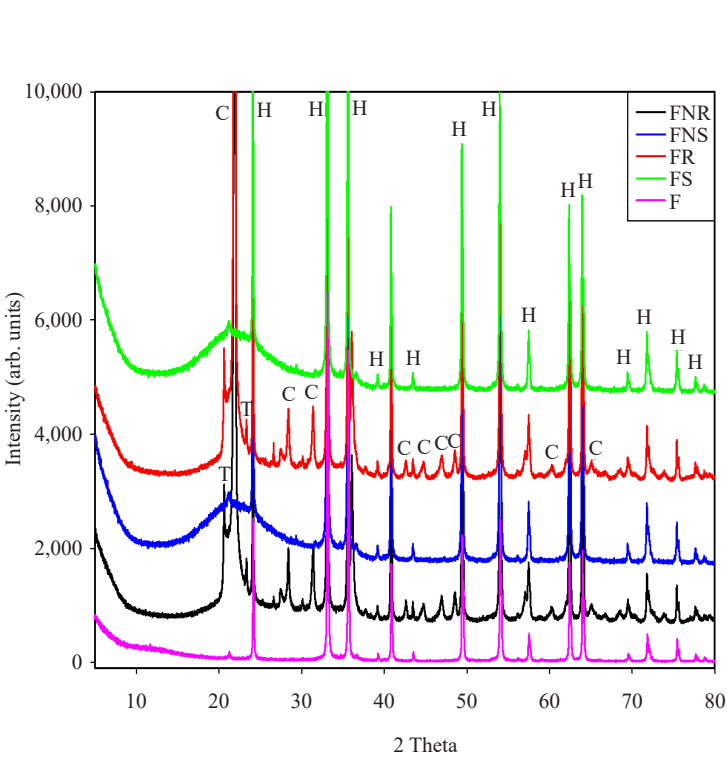


Figure 5. X-ray patterns of ferrisilicates FNR, FNS, FR, and FS. T, C, and H denote peaks of tridymite, cristobalite, and hematite, respectively

3.1.2 Infrared spectra

Figure 6 presents the spectra of kaolin and metakaolin denoted MY3 and MK-MY3, respectively. Absorption bands at 3,618 and 3,685 cm^{-1} , corresponding to the stretching vibration modes of OH bonds, are seen on the spectrum of MY3. These bands can be attributed to the inner and outer hydroxyl groups of the kaolinite, respectively [26]. Absorption bands at 1,613 and 1,624 cm^{-1} on the infrared spectra of kaolin and metakaolin, respectively, are associated with H-O-H vibrational modes of water molecules. The vibrational modes of the Si-O-Al^{VI} and Si-O-Si bonds in the kaolinite structure are associated with those at 1,123 and 1,023 cm^{-1} on the kaolinite spectrum [27], respectively. The deformation of Al^{VI}-OH bonds in the kaolinite structure is ascribed to the peak at 909 cm^{-1} on the kaolinite spectrum [26]. On the spectrum of kaolin, Si-O-Al with Al in VI-fold coordination is assigned to the absorption band that appears at 525 cm^{-1} [28]. The absorption bands at 525, 909, 1,023, 1,123, 3,618, and 3,685 cm^{-1} observed on the spectrum of kaolin disappear in that of metakaolin due to the collapse of the kaolinite structure during calcination. Absorption bands at 909, 1,023, and 1,123 cm^{-1} disappear on the spectrum of kaolin resulting in a broad band at 1,072 cm^{-1} . This band is attributed to the symmetric and asymmetric stretching modes of Si-O-Si and Si-O-Al^{IV} bonds. The disappearance of those at 3,618 and 3,685 cm^{-1} leads to the formation of a broad one at 3,432 cm^{-1} . This corresponds to the stretching vibration modes of OH groups of Si-OH, Al-OH, or H-O-H bonds in the structure of metakaolin. The formation of the broad hump structure appearing between 13 and 35° (2 θ) on the X-ray pattern of metakaolin confirms the formation of broad bands on the infrared spectrum of metakaolin (Figure 3). Absorption bands at 453 and 447 cm^{-1} on the infrared spectra of kaolin and metakaolin, respectively, are assigned to vibrational modes of Si-O bonds. Those at 681 and 784 cm^{-1} are attributed to the Si-O-Si vibrational modes of quartz on the spectra of kaolin and metakaolin, respectively [29].

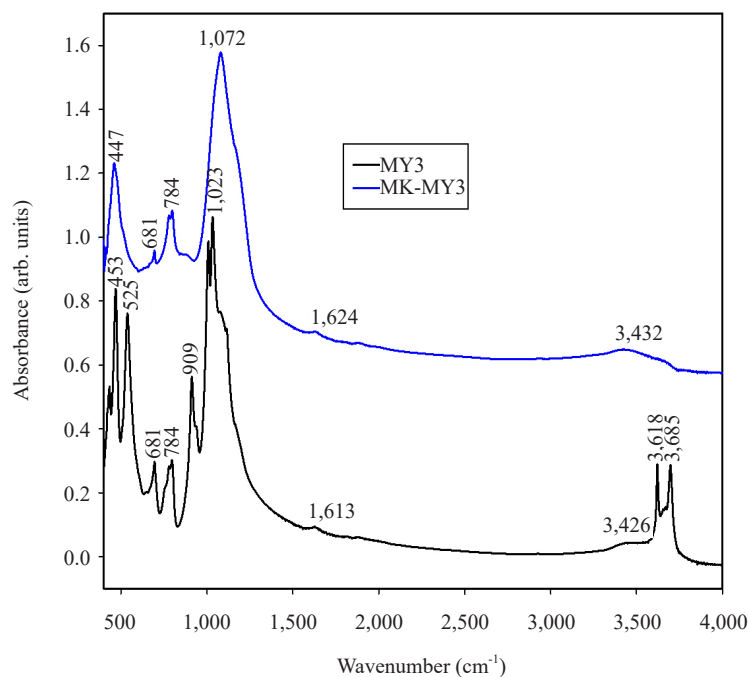


Figure 6. Infrared spectra of kaolin (MY3) and metakaolin (MK-MY3)

Figure 7 depicts the infrared spectra of different ferrisilicates (FNR, FNS, FR, and FS). Infrared spectra of these ferrisilicates are compared to those of commercial hematite. The infrared spectrum of this hematite shows absorption bands at 447 and 552 cm^{-1} . These bands correspond to the bending and stretching vibrations of Fe-O bonds characteristic of hematite. Absorption bands at 552, 570, 547, and 552 cm^{-1} associated with stretching vibrations of Si-O-Fe bonds are

observed on the infrared spectra of the prepared ferrisilicates. These absorption bands are observed on the spectrum of hematite at 552 cm^{-1} (Figure 7). They are not observed on the spectra of silica fume (SF) and rice husk ash (RHA) (Figure 2). This confirmed that Fe atoms from hematite were incorporated into the structure of silica fume and rice husk ash, resulting in the formation of ferrisilicates ($-\text{Si-O-Fe}-$). The absorption bands between 795 and 783 cm^{-1} on the spectra of ferrisilicates are due to the stretching vibrational modes of the Si-O-Si bonds of the amorphous silica contained in their networks. This band is slightly sharper on the spectra of FR and FNR, confirming the presence of crystalline phases such as cristobalite and tridymite in their structures (Figure 5). Due to the higher alkalinity of FNS, a sharp absorption band at 836 cm^{-1} and the band appearing at $1,458\text{ cm}^{-1}$ are attributed to the stretching vibrations of O-C-O of Na_2CO_3 . The higher alkalinity is confirmed by the presence of a strong absorption band at $3,458\text{ cm}^{-1}$, belonging to the stretching vibrations of the OH groups. The absorption band at $1,677\text{ cm}^{-1}$ may be related to the bending vibrations of the H-O-H of water molecules. It is only present on the spectra of the ferrisilicates FNS and FS. This is an indication that FNS and FS may have a strong affinity for water. Absorption bands at $1,085$, $1,061$, $1,091$, and $1,091\text{ cm}^{-1}$ on FNR, FNS, FR, and FS spectra, respectively, are attributed to stretching vibrations of Si-O-Si bonds. On the spectra of silica fume and rice husk ash, these absorption bands appear at $1,103$ and $1,098\text{ cm}^{-1}$, respectively (Figure 2). On the infrared spectra of FNR, FR, FNS, and FS these bands appear to shift to 13 , 7 , 42 , and 6 cm^{-1} , respectively. The shift of these bands towards lower wavenumbers on the infrared spectra of ferrisilicates suggests the incorporation of $\alpha\text{-Fe}_2\text{O}_3$ into the structure of silica fume and rice husk ash. This is due to the dissolution of the amorphous silica present in both silica sources under sodium hydroxide solution and distilled water. Related to the lower hydrolysis of amorphous silica in distilled water is the lower wavenumber shift for FR (7 cm^{-1}) and FS (6 cm^{-1}). This suggests that FR and FS may contain a greater amount of undissolved amorphous silica in their structures. The presence of tridymite and cristobalite may explain the lower dissolution of amorphous silica from rice husk ash in sodium hydroxide solution (Figure 7). This is confirmed by the lower shift of the wavenumber of the main band of 13 cm^{-1} in FNR versus 42 cm^{-1} in FNS.

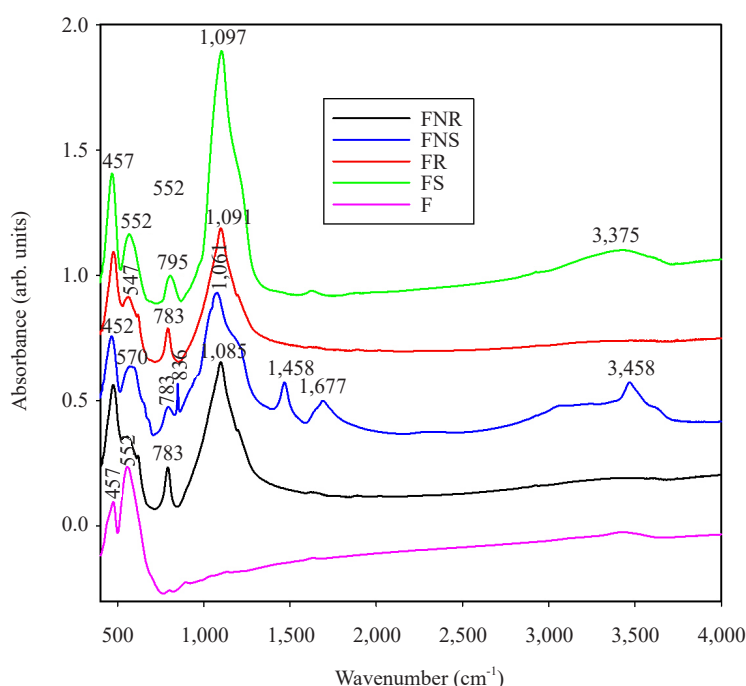


Figure 7. Infrared spectra of ferrisilicates, FNR, FNS, FR, and FS

3.2 Characterizations of metakaolin-based geopolymer composites

3.2.1 Identification of the crystalline phases

The X-ray patterns of the geopolymer composites, GF0, GFNR, GFNS, GFR, and GFS are depicted in Figure 8. Illite, quartz, and anatase peaks are seen on the diffractograms of all geopolymer composites. In addition to these phases, the peaks of hematite, which are compared to the X-ray pattern of commercial hematite, are present on the X-ray patterns of geopolymer composites from the incorporation of FNR, FNS, FR, and FS. The cristobalite peaks appear on the X-ray patterns of the geopolymer composites GFNR and GFR. In addition to these crystalline minerals, the diffractograms show the amorphous phase between 18° and 40° (2θ), due to the formation of binders in the structure of the geopolymer composites. The shift of the broad hump structure appearing between 13 and 35° (2θ) on the X-ray pattern of metakaolin confirms that the microstructure of metakaolin changes during geopolymerisation leading to the formation of geopolymer binders (Figure 3).

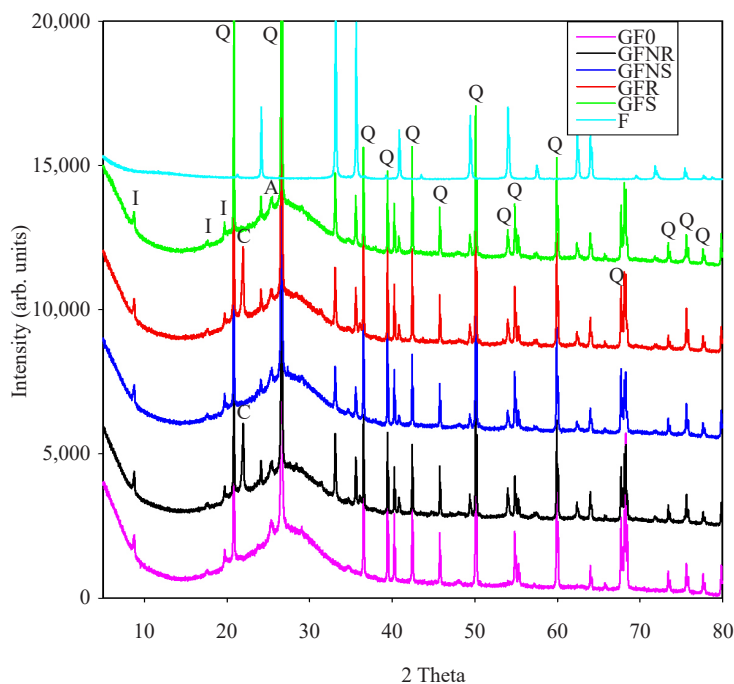


Figure 8. X-ray patterns of hematite (F) and metakaolin-based geopolymer materials GF0, GFNR, GFNS, GFR, and GFS. I, Q, C, and A denote peaks of illite, quartz, cristobalite, and anatase, respectively

3.2.2 Functional group investigations

Figure 9 shows the infrared spectra of geopolymer materials, GF0, GFNR, GFNS, GFR, and GFS, from the incorporation of 0 and 10 wt% of different ferrisilicates, FNR, FNS, FR, and FS. The OH and H-O-H stretching and bending vibrations occur at $3,453$ and $1,640\text{ cm}^{-1}$, respectively. The bending vibrations of Si-O-Si and O-Si-O bonds are assigned to the bands at $464\text{--}440\text{ cm}^{-1}$ [30]–[32]. The symmetric stretching vibrations of Si-O-Si and Al-O-Si are assigned to the weak shoulder band appearing at 552 cm^{-1} [31] and the vibration modes of Fe-O-Si [9], [33]–[37]. The Si-O symmetric bending mode of quartz appears on the infrared spectra of geopolymers at 682 cm^{-1} [29]. The symmetric stretching vibration of Si-O-Al bonds appears on the geopolymer spectrum at 760 cm^{-1} . On the spectra of geopolymer materials, GF0, GFNR, GFNS, and GFR, the symmetric and asymmetric stretching modes of Si-O-Si and Si-O-Al are observed at $1,001\text{ cm}^{-1}$. On the spectrum of GFS, this band is observed at $1,007\text{ cm}^{-1}$. These absorption bands appear

at 1,072 cm^{-1} on the infrared spectrum of metakaolin (Figure 5). The dissolution of metakaolin and the subsequent polycondensation of metakaolin-ferrisilicate composites is responsible for the shift of these absorption bands towards lower wavenumbers on the infrared spectra of geopolymer materials. On the spectra of the geopolymer materials GF0, GFNR, GFNS, and GFR, the same wavenumber values are found in each main absorption band (1,000 cm^{-1}). This suggests that the iron(III) is not incorporated into the network and can probably act as a filler. This indicates that Fe in Fe_2O_3 , acting as filler, surrounds -Si-O-Si-O-Si-O-Si-O-Al- chains. The positions and assignments of the infrared vibration bands of raw materials, ferrisilicates, and geopolymer materials are summarized in Table 2.

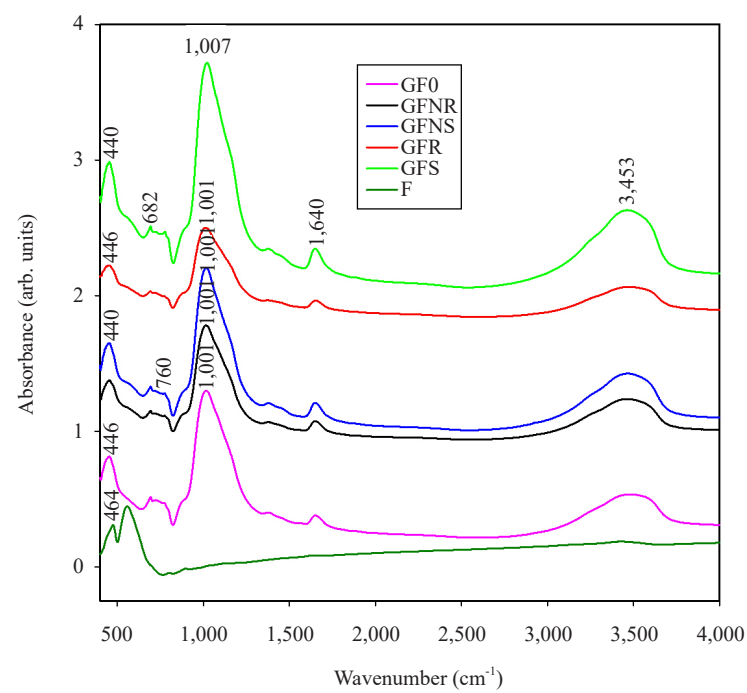


Figure 9. Infrared spectra of hematite (F) and metakaolin-based geopolymer materials GF0, GFNR, GFNS, GFR, and GFS

Table 2. Positions and assignments of the infrared vibration bands of raw materials, ferrisilicates, and geopolymer materials

Positions (cm^{-1})				
MY3	MK-MY3	Ferrisilicates	Geopolymer materials	Assignments
3,618, 3,685	-	-	-	OH groups of kaolinite
3,426	-	-	3,453	OH groups of Si-OH
909	-	-	-	Al-OH
681, 784	681, 784	695, 773	682	Si-O-Si of quartz
1,023	-	1,097-1,067	-	Si-O-Si bonds
784	-	-	-	Si-O-Al ^{VI}

Table 2. (cont.)

Positions (cm ⁻¹)				
MY3	MK-MY3	Ferrisilicates	Geopolymer materials	Assignments
453	447	457	464-440	Si-O-Si bonds
-		570-547		Fe-O bonds
-		836, 1,458		O-C-O
525		-	538	Si-O-Al bonds of illite
-	784	795, 783	760	Si-O-Si of amorphous silica
1,613	1,624, 3,432	1,638, 3,506, 1,677, 3,375, 3,458	1,640, 3,453	H-O-H and O-H of water molecules and silanol groups
-	1,072	1,083	1,007-1,001	Si-O-Si and Si-O-Al ^{IV} bonds

3.2.3 Compressive strength investigations

The compressive strength values of the geopolymer composites GF0, GFNR, GFNS, GFR, and GFS are depicted in Figure 10. As can be seen from this figure, the compressive strength values of the geopolymer composites GF0, GFNR, GFNS, GFR, and GFS are 53.34, 71.91, 77.72, 74.13, and 44.73 MPa, respectively. The highest compressive strength of 77.72 MPa was observed when the ferrisilicate FNS was used as an additive. A minimum compressive strength of 43.73 MPa was achieved when the ferrisilicate FS was added to the metakaolin. The excess of undissolved amorphous silica in its structure, which negatively affects its strength, may be responsible for the lower compressive strength value (43.73 MPa) of GFS. The excess of undissolved amorphous silica in the structure of GFS is confirmed by the lower dissolution of silica fume in ferrisilicate FS. This is confirmed by the lowest wavenumber shift that is observed on the infrared spectrum of the FS (6 cm⁻¹) (Figure 7). The presence of high levels of undissolved silica fume in the structure of geopolymer materials increases the workability of the mix, which limits the contact between metakaolin-FS and sodium water glass and therefore reduces the compressive strength, according to Das et al. [38]. This observation was also made by other investigators such as Wu and Sun [39], Khater [40], Chindaprasirt et al. [41], and Nmiri et al. [42]. Similarly, Khater [43] reported that the excess of undissolved silica fume in the fresh geopolymer materials results in insufficient wetting of the medium, which hinders the propagation of geopolymer material chains and subsequently weakens their compressive strength. In the work of Li and Ou [44], the high content of undissolved silica fume was reported to reduce the compressive strength of geopolymer materials. This makes uniform dispersion difficult and results in the formation of weak zones in the form of voids and hence the heterogeneous microstructure. It was reported by Wang et al. [45] that the excess of unreacted silica fume agglomerated together to form defects, resulting in a reduction in strength. In addition, more unreactive particles can act as stiff fillers. These can cause microcracks in the matrix. This leads to lower compressive strength results [45]. In contrast, less dissolution of the amorphous silica contained in the structure of rice husk ash was observed, but the compressive strength of GFR is higher than that of GF0 and GFS. The higher compressive strength of GFR compared to GF0 and GFS may be explained by the presence of tridymite and cristobalite in its network. These crystalline phases increase the compressive strength of the geopolymers by acting as filling agents. The highest compressive strength values for GFNR (71.91 MPa) and GFNS (77.72 MPa) may be related to the presence of an additional base (Na₂O) in the system. This increases the concentration of NaOH in the sodium silicate and helps to dissolve the mixture of metakaolin-FR and metakaolin-FS composites, thus prolonging the geopolymerisation process.

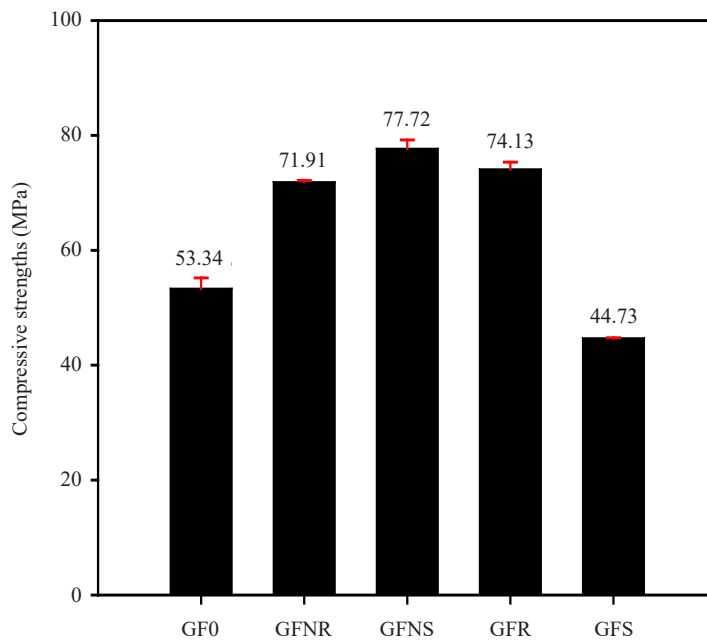
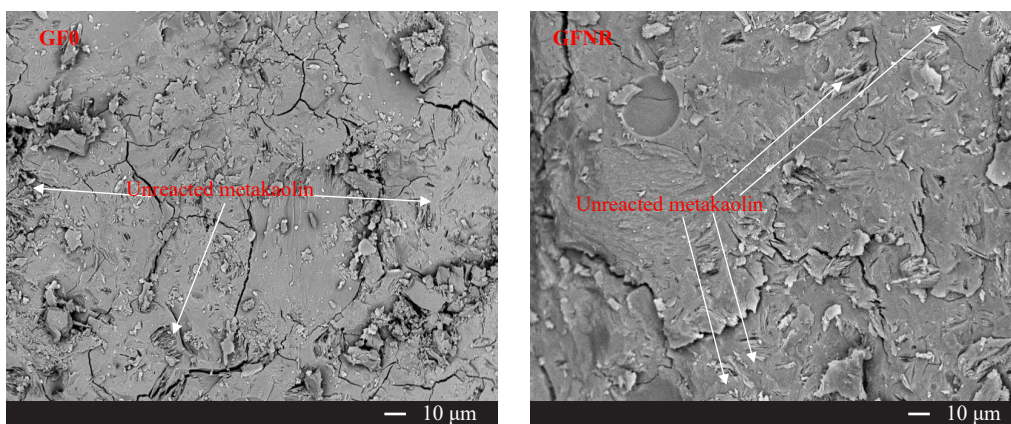


Figure 10. Compressive strengths of metakaolin-based geopolymer materials, GF0, GFNR, GFNS, GFR, and GFS

3.2.4 Micrograph images

The micrograph images of geopolymer materials GF0, GFNR, GFNS, GFR, and GFS are given in Figure 11. The micrographs of these geopolymer materials show a compact, homogeneous, and denser matrix, which is in agreement with the results of the compressive strength tests (Figure 10). The tiny plate-like crystals of metakaolinite can be seen in some of the areas in these micrographs. Melele et al. [46] concluded that unreacted metakaolin particles in geopolymer materials could act as microaggregates and reinforce the network. This could be explained by the high compressive strengths of the geopolymer materials: GF0, GFNR, GFNS, GFR, and GFS, although one of the GFS (44.73 MPa) is lower than the others (Figure 10). Some cracks were observed in the micrographies of the geopolymer materials. These have been attributed to the fracture of the poly(sialate-ferro-siloxo) networks.



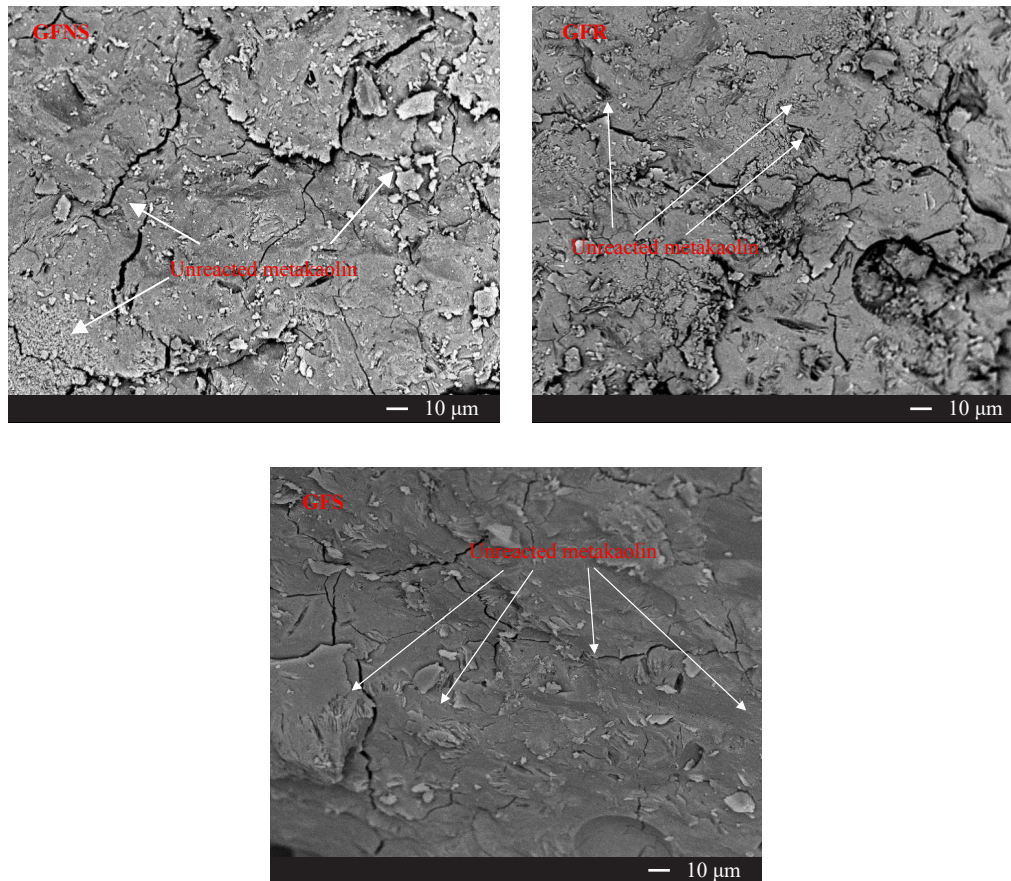
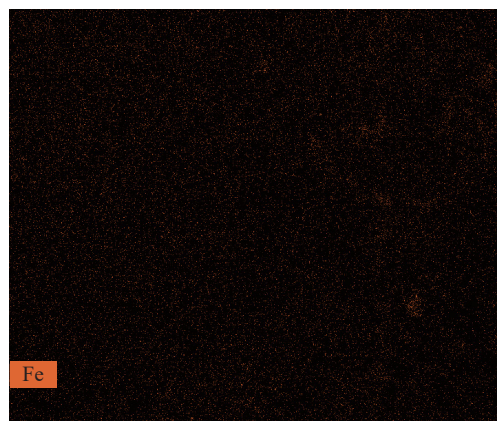
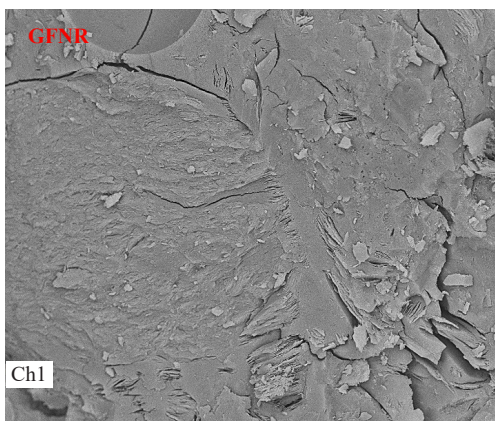
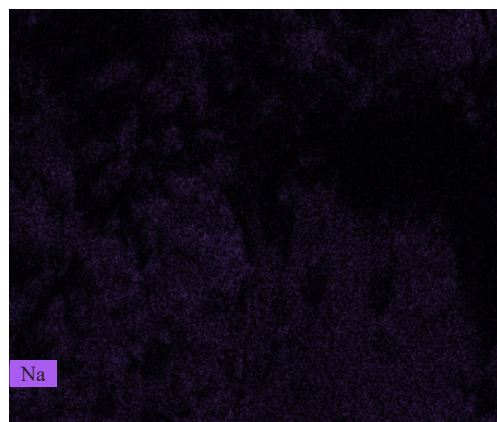
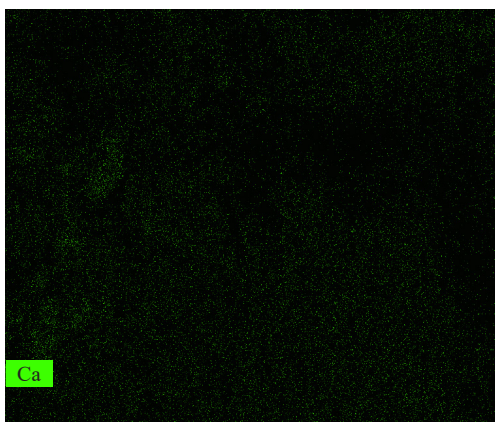
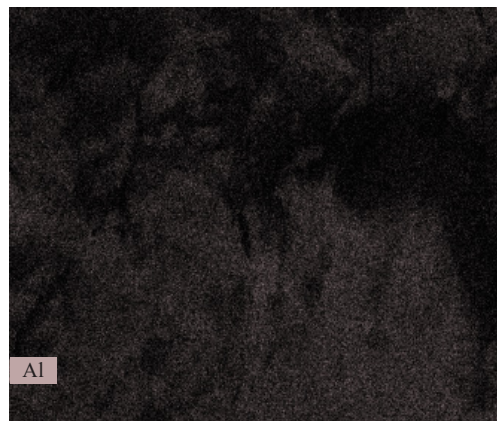
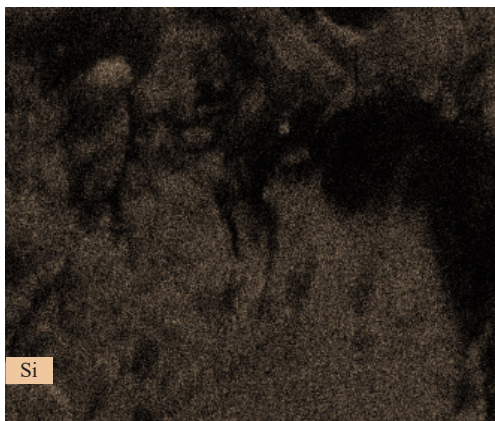
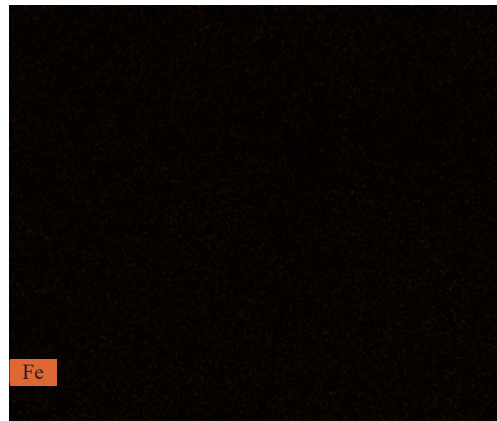
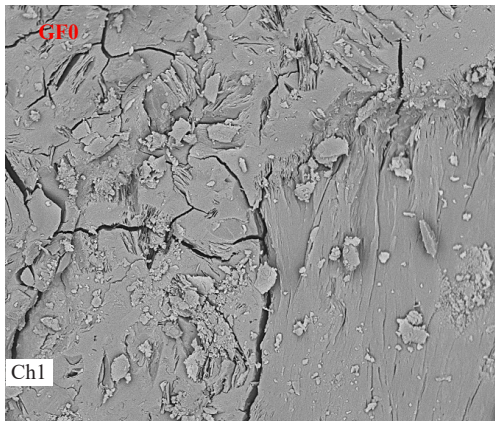
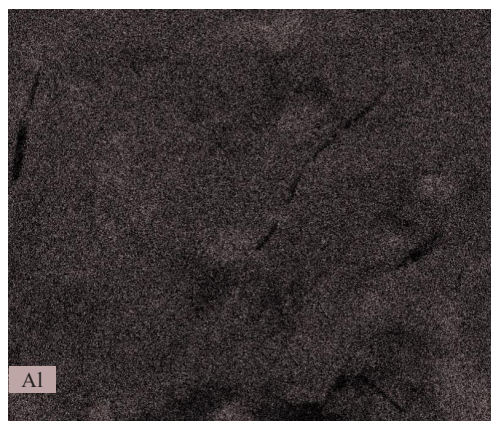
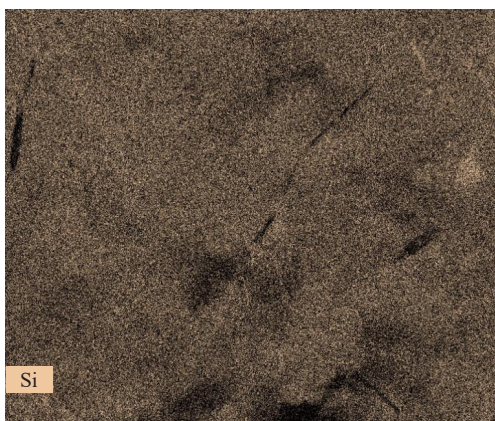
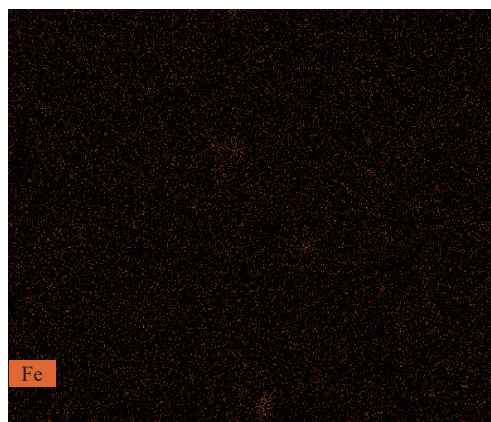
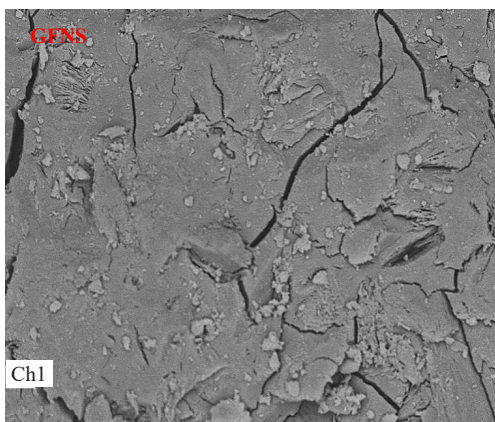
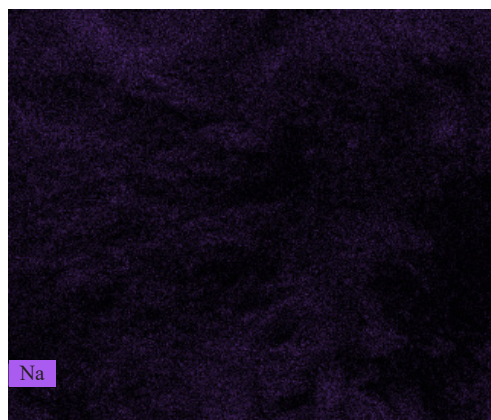
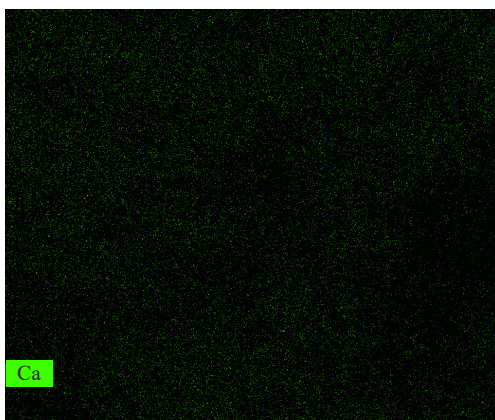
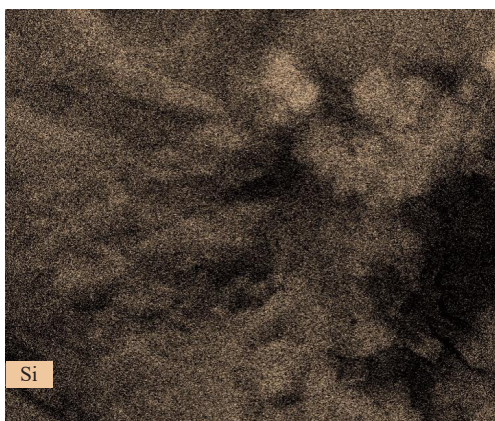


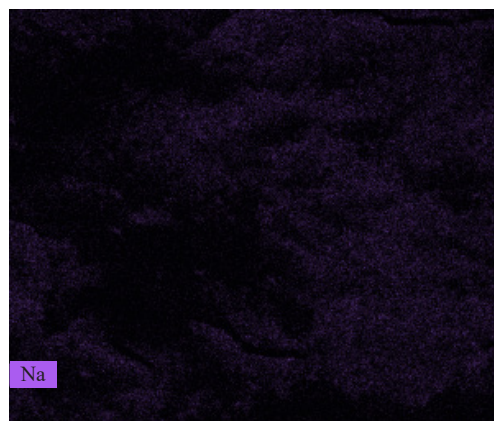
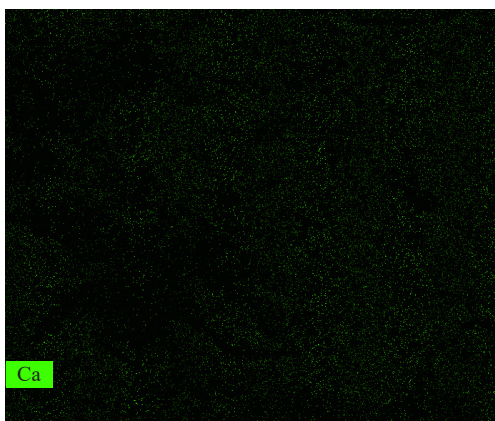
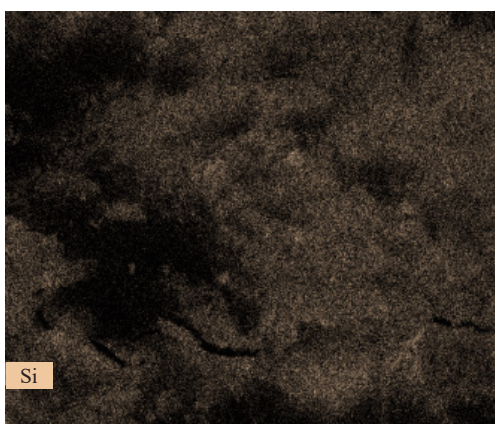
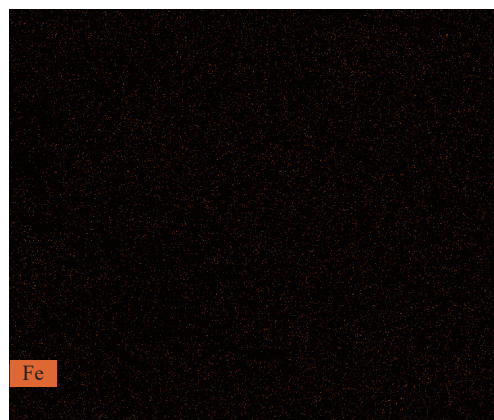
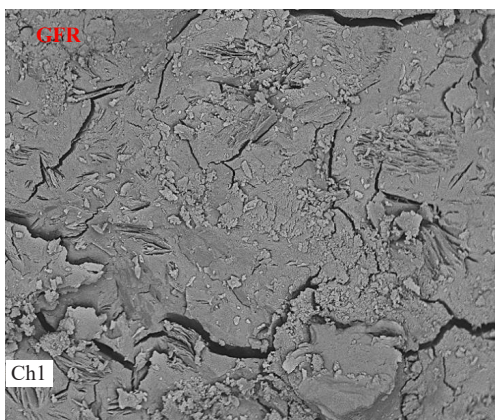
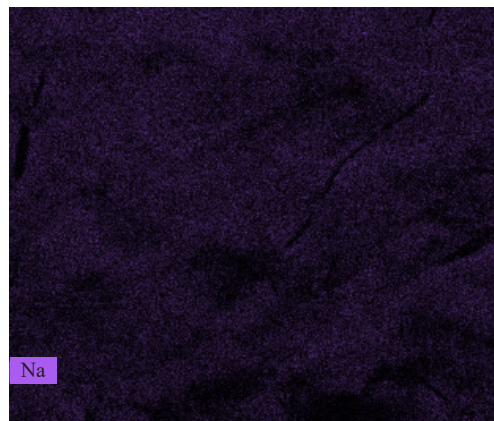
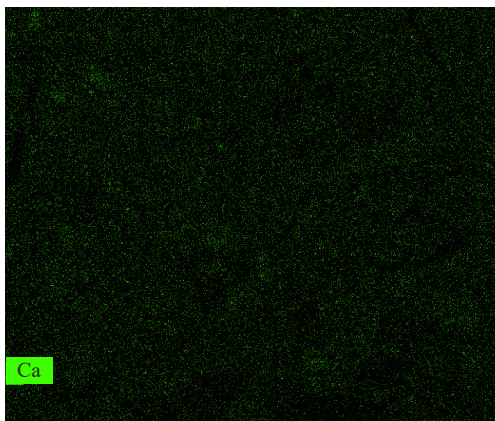
Figure 11. Micrograph images of geopolymer materials GF0, GFNR, GFNS, GFR, and GFS

3.2.5 Elemental distribution investigations

The EDS mapping of Ca, Na, Fe, Si, and Al elements in the geopolymer materials GF0, GFNR, GFNS, GFR, and GFS displayed in Figure 12. This indicates that these elements are well distributed throughout the geopolymer network. The combination of Fe, Si, and Al maps revealed the formation of Fe-O-Si-O-Al. This proved to be one of the most important bonds determining the compressive strength of geopolymer materials. The good distribution of Fe, Si, and Al in the geopolymers indicates that the formation of a homogeneous matrix increases the compressive strength through the filling of the microvoids in the geopolymers with hematite acting as a filler. This is consistent with the compressive strengths of the geopolymer materials GF0, GFNR, GFNS, and GFR. Due to the similar size of Ca^{2+} ($r = 1.00 \text{ \AA}$) and Na^+ ($r = 1.02 \text{ \AA}$), which does not alter the 3D structure of the geopolymer materials, the good distribution of ions such as Ca^{2+} and Na^+ in the geopolymer networks balances the negative charge caused by the substitution of $\text{Al}^{(\text{III})}$ by $\text{Si}^{(\text{IV})}$ and $\text{Al}^{(\text{III})}$ by some Fe(III) [47]. In addition to the nanocrystalline hematite dispersed throughout the matrix of the GF0, GFNR, GFNS, GFR, and GFS geopolymers, samples GFNR and GFNS show some zones where the hematite particles are agglomerated, as regards the distribution of iron(III) in the geopolymer networks. The capillary pores could be filled by these agglomerated hematite particles. Compared to the EDS mapping of GFNR, GFNS, and GFR, which shows a high amount of Si, Si is present in a low amount in the structure of the geopolymer material GFS, as well as Na^+ and Ca^{2+} . This suggests the formation of a more Al-rich geopolymer material, which is responsible for its low compressive strength value (43.73 MPa). This is supported by the results of the work of Fernández-Jiménez et al. [48].







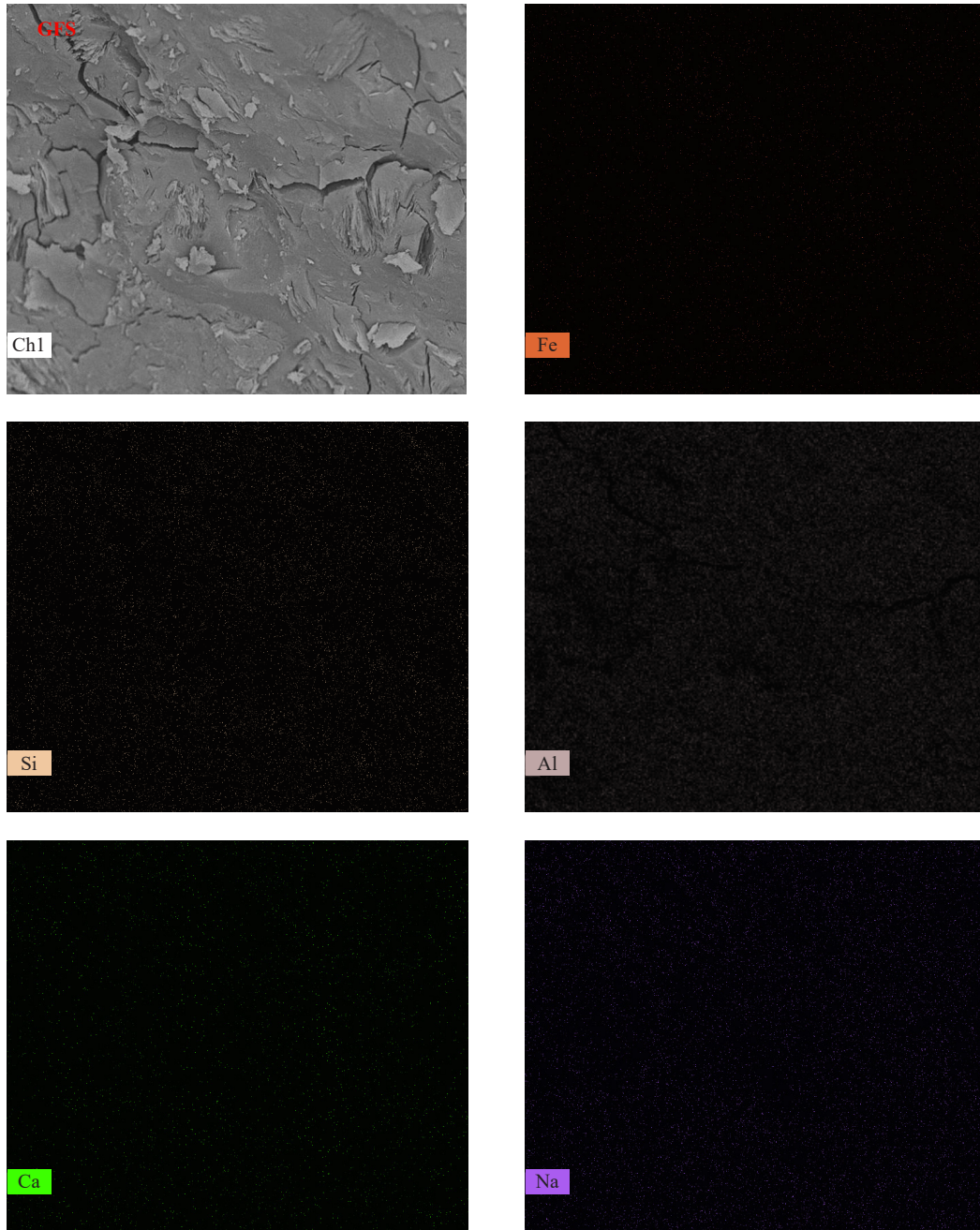


Figure 12. SEM with EDS mapping of Ca, Na, Fe, Si, and Al elements in the geopolymer materials GF0, GFNR, GFNS, GFR, and GFS collected at 1,200x with a $1,500 \times 1,125$ nm step-size over 10 minutes. Ch1 is an area of specimen selected for area mapping

4. Conclusion

Metakaolin, obtained by calcining kaolin at 700 °C, was used as the aluminosilicate source for the synthesis of geopolymer materials, and sodium silicate as the hardener. Rice husk ash and silica fume were used as silica sources and hematite as an iron mineral to produce various ferrisilicates. The $\text{Fe}_2\text{O}_3/\text{SiO}_2$ molar ratio was set at 0.2. Four ferric silicates were prepared in two solvents, sodium hydroxide (2M) and distilled water. To obtain five formulations of geopolymer materials, metakaolin was replaced by 0 and 10 wt% of each ferrisilicate and the four powders obtained were separately mixed with sodium water glass. Studies have been carried out on the functional groups and crystalline

phases of ferrisilicates and geopolymers. The compressive strength, the morphology, and the elemental mapping of the geopolymer materials have been measured. The results obtained show that the compressive strength of the metakaolin-based geopolymer materials without the addition of ferrisilicate is 53.34 MPa. These are 71.91 and 77.72 MPa for the addition of ferrisilicate obtained by dissolving rice husk ash-hematite and silica fume-hematite in sodium hydroxide solution, respectively. In contrast, those from the addition of ferrisilicate, obtained by dissolution of rice husk ash-hematite and silica fume-hematite in distilled water, are 74.13 and 43.73 MPa, respectively. The microstructure shows a homogeneous, compact, and dense geopolymer matrix, although there is some unreacted metakaolin and some cracking. Elemental mapping carried out by EDS confirmed the homogeneity of the prepared geopolymer materials. The iron particles in the geopolymers are well dispersed throughout the matrix. It was found that the compressive strength of metakaolin-based geopolymeric materials made by adding metakaolin with 10 wt% of ferrisilicates (obtained by dissolving rice husk ash-hematite, silica fume-hematite in sodium hydroxide solution) and ferrisilicate (obtained by dissolving rice husk ash-hematite in water) is higher than that of the materials made by using the ferrisilicates obtained from the mixture of silica fume, hematite, and distilled water. The geopolymer materials produced here could be used in building construction based on the results obtained.

Acknowledgement

Pr. Dr. Hervé Tchakouté Kouamo gratefully acknowledges Alexander von Humboldt-Stiftung for financial support for this work under the grant N° KAM/1155741 GFHERMES-P.

Conflict of interest

The authors declare no competing financial interest.

References

- [1] A. Mehta, and R. Siddique, "An overview of geopolymers derived from industrial by-products," *Construction and Building Materials*, vol. 127, pp. 183-198, 2016.
- [2] Y.-M. Liew, C.-Y. Heah, A. B. Mohd Mustafa, and H. Kamarudin, "Structure and properties of clay-based geopolymer cements: a review," *Progress in Materials Science*, vol. 83, pp. 595-629, 2016.
- [3] T. Suwan, and M. Fan, "Effect of manufacturing process on the mechanisms and mechanical properties, of fly ash-based geopolymer in ambient curing temperature," *Materials Manufacturing Processes*, vol. 32, pp. 461-467, 2017.
- [4] D. E. T. Mabah, H. K. Tchakouté, C. H. Rüschler, E. Kamseu, A. Elimbi, and C. Leonelli, "Design of low cost semi-crystalline calcium silicate from biomass for the improvement of the mechanical and microstructural properties of metakaolin-based geopolymer cements," *Materials Chemistry and Physics*, vol. 223, pp. 98-108, 2019.
- [5] H. K. Tchakouté, D. E. T. Mabah, C. H. Rüschler, E. Kamseu, F. Andreola, M. C. Bignozzi, and C. Leonelli, "Preparation of low-cost nano and microcomposites from chicken eggshell, nano-silica and rice husk ash and their utilisations as additives for producing geopolymer cements," *Journal of Asian Ceramic Societies*, vol. 8, pp. 149-161, 2020.
- [6] A. M. N. Moudio, H. K. Tchakouté, D. L. V. Ngnintedem, F. Andreola, E. Kamseu, C. P. Nanseu-Njiki, C. Leonelli, and C. H. Rüschler, "Influence of the synthetic calcium aluminate hydrate and the mixture of calcium aluminate and silicate hydrates on the compressive strengths and the microstructure of metakaolin-based geopolymer cements," *Materials Chemistry and Physics*, vol. 264, pp. 124459, 2021.
- [7] H. I. Riyap, B. K. Ngongang, H. K. Tchakouté, C. P. Nanseu-Njiki, and C. H. Rüschler, "Compressive strengths and microstructural properties of geopolymeric materials arising from the addition of semi-crystalline alumina to silica-rich aluminosilicate sources," *Silicon*, vol. 14, pp. 10535-10558, 2022.
- [8] D. L. V. Ngnintedem, M. Lampe, H. K. Tchakouté, C. H. Rüschler, "Effects of iron minerals on the compressive strengths and microstructural properties of metakaolin-based geopolymer materials," *Gels*, vol. 8, pp. 525, 2022.
- [9] R. Kaze, L. Beleuk à Moungam, M. Cannio, R. Rosa, E. Kamseu, U. Chinje, and C. Leonelli, "Microstructure and

- engineering properties of $\text{Fe}_2\text{O}_3(\text{FeO})\text{-Al}_2\text{O}_3\text{-SiO}_2$ based geopolymer composites,” *Journal of Cleaner Production*, vol. 199, pp. 849-859, 2018.
- [10] E. Kamseu, C. R. Kaze, J. N. N. Fekoua, U. F. C. Melo, S. Rossignol, and C. Leonelli, “Ferrisilicates formation during the geopolymerization of natural Fe-rich aluminosilicate precursors,” *Materials Chemistry and Physics*, vol. 240, pp. 122062, 2020.
 - [11] Q. Zhu, R. M. van Teeffelen, R. A. van Santen, and E. J. M. Hensen, “Effect of high-temperature treatment on Fe/ZSM-5 prepared by chemical vapor deposition of FeCl_3 II. Nitrous oxide decomposition, selective oxidation of benzene to phenol, and selective reduction of nitric oxide by isobutene,” *Journal of Catalysis*, vol. 221, no. 2, pp. 575-583, 2004.
 - [12] E. J. M. Hensen, Q. Zhu, M. M. R. M. Hendrix, A. R. Overweg, P. J. Kooyman, M. V. Sychev, and R. A. van Santen, “Effect of high-temperature treatment on Fe/ZSM-5 prepared by chemical vapor deposition of FeCl_3 I. Physicochemical characterization,” *Journal of Catalysis*, vol. 221, pp. 560-574, 2004.
 - [13] G. P. Glasby, and H. D. Schulz, “Eh-Ph diagrams for Mn, Fe, Co, Ni, Cu and as under seawater conditions: Application of two new types of eh ph diagrams to the study of specific problems in marine geochemistry,” *Aquatic Geochemistry*, vol. 5, pp. 227-248, 1999.
 - [14] K. K. Kefeni, T. A. Msagati, T. T. Nkambule, and B. B. Mamba, “Synthesis and application of hematite nanoparticles for acid mine drainage treatment,” *Journal of Environmental Chemical Engineering*, vol. 6, pp. 1865-1874, 2018.
 - [15] D. Adak, M. Sarkar, and S. Mandal, “Structural performance of nano-silica modified fly-ash based geopolymer concrete,” *Construction and Building Materials*, vol. 135, pp. 430-439, 2007.
 - [16] P. Duan, C. Yan, and W. Zhou, “Compressive strength and microstructure of fly ash based geopolymer blended with silica fume under thermal cycle,” *Cement and Concrete Composites*, vol. 78, pp. 108-119, 2017.
 - [17] G. Saini, U. Vattipalli, “Assessing properties of alkali activated GGBS based self-compacting geopolymer concrete using nano-silica,” *Case Studies in Construction Materials*, vol. 12, pp. 352, 2020.
 - [18] Y. Liu, C. Shi, Z. Zhang, N. Li, and D. Shi, “Mechanical and fracture properties of ultra-high performance geopolymer concrete: Effects of steel fiber and silica fume,” *Cement and Concrete Composites*, vol. 112, pp. 103665, 2020.
 - [19] S. J. K. Melele, H. K. Tchakouté, C. Banenzoué, E. Kamseu, C. H. Rüschler, F. Andreola, and C. Leonelli, “Investigation of the relationship between the condensed structure and the chemically bonded water content in the poly(sialate-siloxo) network,” *Applied Clay Science*, vol. 156, pp. 77-86, 2018.
 - [20] P. M. Dove, N. Han, A. F. Wallace, and J. J. De Yoreo, “Kinetics of amorphous silica dissolution and the paradox of the silica polymorphs,” *Proceedings of the National Academy of Sciences*, vol. 105, pp. 9903-9908, 2008.
 - [21] P. Ptáček, D. Kubátová, J. Havlica, J. Brandstetr, F. Soukal, and T. Opravil, “Isothermal kinetic analysis of the thermal decomposition of kaolinite: The thermogravimetric study,” *Thermochimica Acta*, vol. 501, pp. 24-29, 2010.
 - [22] P. Ptáček, F. Šoukal, T. Opravil, M. Noskova, J. Havlica, and J. Brandštetr, “The kinetics of Al-Si spinel phase crystallization from calcined kaolin,” *Journal of Solid State Chemistry*, vol. 183, pp. 2565-2569, 2010.
 - [23] S. Sperinck, P. Raiteri, N. Marks, and K. Wright, “Dehydroxylation of kaolinite to metakaolin-a molecular dynamics study,” *Journal of Materials Chemistry*, vol. 21, pp. 2118-2125, 2011.
 - [24] P. Ptáček, F. Šoukal, T. Opravil, J. Havlica, and J. Brandštetr, “Crystallization of spinel phase from metakaoline: the nonisothermal thermodilatometric CRH study,” *Powder Technology*, vol. 243, pp. 40-45, 2013.
 - [25] B. Li, J. Xu, J. Liu, S. Zuo, Z. Pan, and Z. Wu, “Preparation of mesoporous ferrisilicate with high content of framework iron by pH-modification method and its catalytic performance,” *Journal of Colloid and Interface Science*, vol. 366, pp. 114-119, 2012.
 - [26] B. J. Saikia, and G. Parthasarathy, “Fourier transform infrared spectroscopic characterization of kaolinite from Assam and Meghalaya, northeastern India,” *Journal of Modern Physics*, vol. 1, no 4, pp. 206-210, 2010.
 - [27] A. M. Qtaitat, and N. I. Al-Trawnet, “Characterization of kaolinite of the Baten El-Ghoulregion/south Jordan by infrared spectroscopy,” *Spectrochimica Acta A*, vol. 61, pp. 1519-1523, 2005.
 - [28] A. Tironi, M. A. Trezza, E. F. Irassar, and A. N. Scian, “Thermal treatment of kaolin: Effect on the pozzolanic activity,” *Procedia Materials Science*, vol. 1, pp. 343-350, 2012.
 - [29] H. K. Tchakouté, C. H. Rüschler, J. N. Y. Djobo, B. B. D. Kenne, and D. Njopwouo, “Influence of gibbsite and quartz in kaolin on the properties of metakaolin-based geopolymer cements,” *Applied Clay Science*, vol. 107, pp. 188-194, 2015.
 - [30] W. K. W. Lee, and J. S. J. van Deventer, “The effect of ionic contaminants on the early-age properties of alkali-activated fly ash-based cements,” *Cement and Concrete Research*, vol. 32, pp. 577-584, 2002.
 - [31] D. Panias, I. P. Giannopoulou, and T. Perraki, “Effect of synthesis parameters on the mechanical properties of fly

- ash-based geopolymers,” *Colloids and Surface A: Physicochemical Engineering Aspects*, vol. 301, pp. 246-254, 2007.
- [32] A. M. M. Al Bakri, K. Hussin, M. Bnhussain, K. N. Ismail, Z. Yahya, and R. A. Razak, “Fly ash-based geopolymer lightweight concrete using foaming agent,” *International Journal of Molecular Sciences*, vol. 13, pp. 7186-7198, 2012.
- [33] H. D. Ruan, R. L. Frost, and J. T. Klopogge, “Infrared spectroscopy of goethite dehydroxylation: III. FT-IR microscopy of in situ study of the thermal transformation of goethite to hematite,” *Spectrochimica Acta Part A Molecular and Biomolecular Spectroscopy*, vol. 8, pp. 967-981, 2002.
- [34] E. M. Moreno, M. Zayat, M. P. Morales, C. J. Serna, A. Roig, and D. Levy, “Preparation of narrow size distribution superparamagnetic $\gamma\text{-Fe}_2\text{O}_3$ nanoparticles in a sol-gel transparent SiO_2 matrix,” *Langmuir*, vol. 18, pp. 4972-4978, 2002.
- [35] R. Kaze, L. Beleuk à Moungam, M. F. Djouka, A. Nana, E. Kamseu, U. C. Melo, and C. Leonelli, “The corrosion of kaolinite by iron minerals and the effects on geopolymerization,” *Applied Clay Science*, vol. 138, pp. 48-62, 2017.
- [36] R. Nkwaju, J. Djobo, J. Nouping, P. Huisken, J. Deutou, and L. Courard, “Iron-rich laterite-bagasse fibers based geopolymer composite: Mechanical, durability and insulating properties,” *Applied Clay Science*, vol. 183, pp. 105333, 2019.
- [37] A. G. Mimboe, M. T. Abo, J. N. Y. Djobo, S. Tome, R. C. Kaze, and J. G. N. Deutou, “Lateritic soil based-compressed earth bricks stabilized with phosphate binder,” *Journal of Building Engineering*, vol. 31, pp. 101465, 2020.
- [38] S. K. Das, S. M. Mustakim, A. Adesina, J. Mishra, T. S. Alomayri, H. S. Assaedi, and C. R. Kaze, “Fresh, strength and microstructure properties of geopolymer concrete incorporating lime and silica fume as replacement of fly ash,” *Journal of Building Engineering*, vol. 32, pp. 101780, 2020.
- [39] H. C. Wu, and P. Sun, “Effect of mixture compositions on workability and strength of fly ash-based inorganic polymer mortar,” *ACI Materials Journal*, vol. 107, no. 6, pp. 554-561, 2010.
- [40] H. M. Khater, “Effect of silica fume on the characterization of the geopolymer materials,” *International Journal of Advanced Structural Engineering*, vol. 5, pp. 1-10, 2013.
- [41] P. Chindaprasart, P. Paisitsrisawat, and U. Rattanasak, “Strength and resistance to sulfate and sulfuric acid of ground fluidized bed combustion fly ash-silica fume alkali-activated composite,” *Advanced Powder Technology*, vol. 25, pp. 1087-1093, 2014.
- [42] A. Nmiri, M. Duc, N. Hamdi, O. Yazoghli-Marzouk, and E. Srasra, “Replacement of alkali silicate solution with silica fume in metakaolin-based geopolymers,” *International Journal of Minerals, Metallurgy and Materials*, vol. 26, pp. 555-564, 2019.
- [43] H. M. Khater, “Physicomechanical properties of nano-silica effect on geopolymer composites,” *Journal of Building Materials Structures*, vol. 3, pp. 1-14, 2016.
- [44] H. Li, H. G. Xiao, and J. P. Ou, “A study on mechanical and pressure-sensitive properties of cement mortar with nanophase materials,” *Cement and Concrete Research*, vol. 34, pp. 435-438, 2004.
- [45] F. Wang, X. Sun, Z. Tao, and Z. Pan, “Effect of silica fume on compressive strength of ultra-high-performance concrete made of calcium aluminate cement/fly ash based geopolymer,” *Journal of Building Engineering*, vol. 62, pp. 105398, 2022.
- [46] S. J. K. Melele, H. K. Tchakouté, C. Banenzoué, E. L. Hseumou, C. P. Nanseu-Njiki, and C. H. Rüschler, “Pore analysis and the behaviour of the unreacted metakaolin particles in the networks of geopolymer cements using metakaolins from kaolinitic and halloysitic clays,” *Silicon*, vol. 14, pp. 2235-2247, 2022.
- [47] I. García-Lodeiro, A. Fernández-Jiménez, A. Palomo, and D. E. Macphée, “Effect of calcium additions on N-A-S-H cementitious gels,” *Journal of the American Ceramic Society*, vol. 93, pp. 1934-1940, 2010.
- [48] A. Fernández-Jiménez, A. Palomo, I. Sobrados, and J. Sanz, “The role played by the reactive alumina content in the alkaline activation of fly ashes,” *Microporous Mesoporous Materials*, vol. 91, pp. 111-119, 2006.